Research Square

Preprints are preliminary reports that have not undergone peer review.
They should not be considered conclusive, used to inform clinical practice,
or referenced by the media as validated information.

Frustration-mediated structural-state selection tunes ionic conductivity in confined polymer--ionic liquid materials

SATOSHI OKAMOTO

satoshi.okamoto.fv@riken.jp

RIKEN: Rikagaku Kenkyujo https://orcid.org/0009-0008-3901-6882

Justin Llandro

Sumitomo Chemical Co., Ltd.

Junko Ikeda

Mageleka Japan Co., Ltd.

Leonid Grunin

Resonance Systems GmbH

Article

Keywords:

Posted Date: August 11th, 2026

DOI: https://doi.org/10.21203/rs.3.rs-10631242/v1

License: This work is licensed under a Creative Commons Attribution 4.0 International License.
Read Full License

Additional Declarations: Yes there is potential Competing Interest. S.O. is an inventor on a patent application related to the materials described in this work. All other authors declare no competing interests.

Abstract

Structural order and ionic transport are usually regarded as competing requirements in solid ionic materials, because crystallization suppresses the molecular motions that enable ion conduction. While confinement is known to alter the phase behavior of ionic liquids, it remains unclear whether competing ordering tendencies in host polymers and confined ionic liquids merely generate unusual ordered phases or instead select the structural state that governs transport.

Here, we identify two distinct structural and transport responses in confined polymer–ionic liquid materials that are consistent with frustration-mediated state selection. By combining crystalline poly(m-benzamide) (pMBA) or amorphous poly(m-oxybenzoate) (pMOB) with 1-butyl-3-methylimidazolium ionic liquids containing either PF_6^- or FSI^-, we systematically vary the polymer host and ionic-liquid anion across four composite systems. Structural analysis reveals two distinct modes through which frustration is accommodated. In pMBA-PF_6, pMOB-PF_6 and pMOB–FSI, thermally persistent ordered diffraction features are observed. In contrast, pMBA–FSI exhibits strongly suppressed diffraction features attributable to long-range polymer and ionic ordering, yielding a thermally robust predominantly amorphous state.

This predominantly amorphous state exhibits the highest ionic conductivity in the series, 3.7×10^{-4} S cm^{-1} at 30°C, despite retaining less ionic liquid than pMOB–FSI, the composite with the highest retained ionic-liquid content.

These results establish structural-state selection as a governing variable for ionic transport in confined polymer–ionic liquid materials. We propose that competing polymer- and ionic-liquid-derived ordering tendencies are accommodated through two distinct pathways: the formation of thermally persistent ordered ionic domains or the suppression of long-range order into a frustrated amorphous state. In the present series, the latter pathway is uniquely realized in pMBA–FSI and yields the highest ionic conductivity despite its intermediate ionic-liquid content, establishing frustration-mediated structural-state selection as a design principle for controlling the order–mobility trade-off in confined ionic materials.

Introduction

Ionic liquids (ILs) are attractive solid-state ionic materials owing to their intrinsic ionic conductivity, negligible vapor pressure, and wide electrochemical stability windows.[1–3] In most ionic materials, however, structural order and ionic transport are generally regarded as competing properties. Crystallization enhances structural stability but suppresses the molecular motions required for ion conduction, whereas disordered states typically facilitate ion transport at the expense of structural order.[4–9] Understanding how structural order and ionic mobility can coexist therefore remains a central challenge in the design of solid-state ionic materials.

Confinement has emerged as a powerful strategy for modifying the structure and dynamics of ionic liquids.[10–15] Previous studies demonstrated that geometric confinement in nanoporous materials and carbon nanotubes can stabilize crystalline ionic-liquid phases that are absent in the bulk state.[16] Similarly, chemically mediated confinement in polymeric systems can induce ionic ordering through specific intermolecular interactions.[17] Although these studies establish that confinement can alter ionic-liquid phase behavior, the resulting ordered states generally remain subject to the conventional trade-off between crystallinity and molecular mobility. However, when ionic liquids are confined within frustrated polymer hosts, the resulting energy landscape is shaped by multiple, competing ordering tendencies originating from both components. It is therefore not obvious whether confinement merely stabilizes unusual ordered ionic states, or whether frustration acts as a state-selection mechanism that determines which structural state, ordered or amorphous, the system ultimately adopts.

Recently, we reported that confinement within meta-linked aromatic polymers produces an unusual ordered ionic-liquid state that retains long-range diffraction order while exhibiting no detectable melting transition over a broad temperature range.[18]

The confined ionic phase remained structurally ordered far beyond the melting behavior of the corresponding bulk ionic liquid and retained finite ionic conductivity despite the apparent absence of a conventional thermodynamic transition.

These observations suggested that meta-linked polymer confinement can generate a frustration-dominated energy landscape that fundamentally alters the ordering pathways available to confined ionic liquids.

However, the previous study was limited to a single polymer–ionic liquid combination and therefore could not determine the broader role of frustration in confined ionic systems.

In particular, it remains unclear whether frustration merely stabilizes unusual ordered ionic states, or whether it actively governs the structural state ultimately selected by the system when multiple competing ordering tendencies are present.

A potential source of such competition arises from the coexistence of polymer-derived and ionic-liquid-derived frustration.

Meta-linked aromatic polymers inherently possess packing constraints originating from their non-linear backbone topology, which inhibits efficient chain packing and generates structurally heterogeneous local environments.[11, 12, 14, 19, 20]

At the same time, ionic liquids are intrinsically susceptible to frustration because of charge ordering, steric asymmetry, conformational flexibility, and competing intermolecular interactions.[2, 4–6]

When ionic liquids are confined within meta-linked polymers, both components may therefore contribute independent sources of frustration.

Here, we test this hypothesis using polymer–ionic liquid composites based on crystalline poly(m-benzamide) (pMBA), amorphous poly(m-oxybenzoate) (pMOB), and ionic liquids containing PF_6^- and FSI^- anions.

By comparing four polymer-ionic liquid composites that differ in polymer host and ionic-liquid anion, we identify two distinct structural responses. Three composites exhibit ordered diffraction features, whereas pMBA–FSI exhibits a predominantly amorphous diffraction profile with strongly suppressed long-range diffraction features.

These results show that ionic conductivity in the present series is not explained by crystallinity or retained ionic-liquid content alone and is associated with the structural state of the composite.

These observations motivate frustration-mediated state selection as a framework for interpreting structural-state selection and ionic conductivity in confined ionic materials.

Results

1. Structural Design and Initial Structural Responses

To investigate how polymer topology and ionic-liquid ordering tendency influence structural organization, a series of polymer-ionic liquid composites was prepared using the phase-change polymerization (PCP) approach previously developed for meta-linked aromatic polymers.

Two meta-linked aromatic polymers with distinct structural characteristics were employed as host matrices. Poly(m-benzamide) (pMBA) forms a crystalline structure through intermolecular hydrogen bonding, whereas poly(m-oxybenzoate) (pMOB) remains predominantly amorphous because the ether linkage suppresses efficient chain packing. The structural states of the neat polymers were confirmed by PXRD prior to composite preparation (Figure S1).

To systematically vary the ordering tendency of the ionic-liquid component, two ionic liquids sharing the same 1-butyl-3-methylimidazolium ($BMIM^+$) cation but containing different anions were selected. BMIM–PF_6 is known to readily develop ordered ionic structures, whereas BMIM–FSI contains the conformationally flexible FSI− anion, which reduces the tendency toward long-range ionic ordering.

The monomers were polymerized in the presence of the ionic liquids at 200°C for 24 h. The resulting powders were washed thoroughly with methanol to remove residual monomers and unbound ionic liquid, followed by vacuum drying to afford polymer–ionic liquid composites. This procedure yielded four model systems: pMBA–PF_6, pMOB–PF_6, pMBA–FSI, and pMOB–FSI (Fig. 1a). The retention of PF_6-containing ionic liquid after washing was further confirmed by XRF measurements through the observation of characteristic phosphorus signals (Figure S2).

These systems provide a comparative platform for examining how polymer-host characteristics and ionic-liquid anion chemistry are associated with structural evolution in polymer–ionic liquid composites.

SEM observations revealed micron-sized particulate morphologies for all polymer–ionic liquid composites, with no evidence of macroscopic phase separation (Figure S3).

The structural responses of the resulting composites were first examined by powder X-ray diffraction (PXRD) (Fig. 1b). The diffraction patterns revealed markedly different structural states depending on the polymer–ionic liquid combination. Distinct diffraction peaks associated with ordered ionic structures were observed for pMBA–PF_6, pMOB–PF_6, and pMOB–FSI, indicating the development of long-range ordering within the confined ionic-liquid domains. Notably, such ordering emerged in both crystalline and amorphous polymer matrices, suggesting that the formation of ordered ionic domains is not determined solely by the initial structural state of the host polymer.

In contrast, pMBA–FSI exhibited fundamentally different behavior. The diffraction features associated with both polymer crystallinity and ionic-liquid ordering were substantially suppressed, resulting in a predominantly amorphous diffraction profile. This observation indicates that the pMBA–FSI combination does not develop the long-range diffraction order observed in the other composites.

These results demonstrate that the structural evolution of polymer–ionic liquid composites depends strongly on the specific combination of polymer topology and ionic-liquid chemistry. While three systems evolve toward states containing ordered ionic domains, the pMBA–FSI system adopts a structurally distinct amorphous state. The thermal stability of these structurally different states was therefore investigated by variable-temperature X-ray diffraction measurements.

2. Thermal Persistence of the Structural States

To examine the thermal stability of the structural states identified by room-temperature PXRD, variable-temperature PXRD (VT-PXRD) measurements were performed for the four polymer–ionic liquid composites (Fig. 2). The diffraction patterns were recorded from room temperature to temperatures exceeding the glass-transition region of the host polymers.

Variable-temperature powder X-ray diffraction (VT-PXRD) patterns of (a) pMBA–PF6, (b) pMOB–PF6, (c) pMBA–FSI, and (d) pMOB–FSI recorded during heating from 30 to 320°C. The diffraction peaks observed for pMBA–PF_6 and pMOB–PF_6 remain detectable throughout the investigated temperature range, indicating the persistence of ordered structures under thermal activation. In pMOB–FSI, several diffraction peaks remain detectable upon heating, although some diffraction features gradually weaken or disappear. In contrast, pMBA–FSI maintains a predominantly amorphous diffraction profile without the emergence of distinct diffraction peaks upon heating.

These results demonstrate that the structural states selected in each composite are thermally robust: systems exhibiting ordered structures remain ordered, whereas the pMBA–FSI composite retains its amorphous character over a broad temperature range.

The composites exhibiting ordered diffraction features at room temperature showed different degrees of thermal persistence upon heating. pMBA–PF_6 and pMOB–PF_6 retained their characteristic diffraction

peaks throughout the investigated temperature range. In pMOB–FSI, several diffraction peaks remained detectable at elevated temperatures, although other diffraction features gradually weakened or disappeared. Nevertheless, the diffraction profile remained distinct from that of the amorphous pMBA–FSI system, indicating partial retention of ordered structural features.

Although shifts in diffraction angle and changes in peak intensity were observed upon heating, no evidence of a major structural transformation or the emergence of a new diffraction pattern was detected. The ordered structural features observed at room temperature were largely preserved, although their thermal persistence depended on the polymer–ionic liquid combination.

A markedly different behavior was observed for pMBA–FSI. In this system, the broad amorphous diffraction profile remained essentially unchanged during heating from 30 to 320°C. No distinct diffraction peaks attributable to either polymer crystallization or ionic-liquid ordering emerged upon heating. The absence of thermally induced ordering during heating from 30 to 320°C indicates that the predominantly amorphous state is structurally persistent over this experimental temperature range.

Notably, all four systems retained the structural character established at room temperature despite thermal activation above the glass-transition region. Composites exhibiting ordered diffraction features at room temperature retained at least part of their characteristic ordered structural features upon heating, whereas the amorphous pMBA–FSI composite remained amorphous throughout the investigated temperature range.

These results indicate that the structural responses identified in Fig. 1 persist during the VT-PXRD heating experiments from 30 to 320°C. To further examine the thermal signatures associated with these structurally distinct states, differential scanning calorimetry was subsequently performed.

3. Thermal Signatures of Structurally Distinct Composite States

Differential scanning calorimetry (DSC) was performed to examine the thermal behavior of the four polymer–ionic liquid composites and to further assess the stability of the structural states identified by PXRD (Fig. 3).

Differential scanning calorimetry (DSC) thermograms of pMBA–PF_6, pMOB–PF_6, pMBA–FSI, and pMOB–FSI. Thermal events associated with the glass transition of the polymer-rich phase are observed depending on the composite composition. In contrast, no pronounced endothermic or exothermic peaks attributable to melting, crystallization, or other large-scale structural transformations are detected within the investigated temperature range.

These thermal characteristics are consistent with the VT-PXRD results shown in Fig. 2, indicating that the structural states established in each composite remain largely unchanged upon heating. Composites exhibiting ordered diffraction features retain substantial portions of their ordered structural characteristics upon heating, whereas the pMBA–FSI system remains predominantly amorphous throughout the investigated temperature range.

The DSC thermograms revealed clear differences in thermal response among the composites, while also demonstrating the absence of major thermally induced structural transitions within the investigated temperature range. For comparison, the thermal behavior of the corresponding neat polymers was examined separately (Figure S4).

Glass-transition behavior was observed in some composites depending on the polymer–ionic liquid combination, indicating thermally activated segmental motion within the polymer-rich phase. The observed thermal responses varied according to the specific polymer–ionic liquid combination, reflecting differences in polymer–ionic liquid interactions and local structural organization.

Despite the occurrence of glass transitions, no pronounced melting endotherms corresponding to extensive crystallization–melting transitions were observed in the composites. In particular, the pMBA–FSI system did not exhibit thermal events indicative of the formation or disappearance of ordered phases, consistent with its predominantly amorphous diffraction profile observed by PXRD. Similarly, the ordered states observed in pMBA–PF_6, pMOB–PF_6, and pMOB–FSI remained free of large thermally induced phase transitions.

These thermal characteristics are consistent with the VT-PXRD results shown in Fig. 2. Although thermal activation above the glass-transition region increases polymer segmental mobility, the structural states selected in each composite remain largely unchanged. Ordered composites retain their ordered character, whereas the pMBA–FSI system remains predominantly amorphous throughout the investigated temperature range.

The absence of major thermal transformations suggests that the distinct structural states identified in Fig. 1 represent thermally persistent configurations rather than transient intermediates. The influence of these structurally distinct states on ionic transport was therefore examined by electrochemical impedance spectroscopy.

4. Ionic transport and conductivity in polymer–ionic liquid composites

Because EIS measurements were performed using hot-pressed composite sheets, the effect of the pressing procedure on the structural state was examined. PXRD patterns collected before and after hot pressing at 260°C showed no substantial changes in the diffraction profiles of the composites. Notably, pMBA–FSI retained its broad predominantly amorphous diffraction profile after pressing, showing that its PXRD-resolved structural signature was retained during EIS sample preparation. To investigate how the distinct structural states identified above influence ion transport, electrochemical impedance spectroscopy (EIS) measurements were performed for the polymer–ionic liquid composites (Fig. 4).

These results demonstrate that ionic conductivity and impedance response vary strongly among the polymer–ionic liquid composites. The impedance response depends strongly on the polymer host, whereas the ionic-conductivity trend is associated with the structural state developed within the composite.

The Nyquist plots revealed markedly different transport characteristics depending on the polymer–ionic liquid combination. The pMOB–PF_6 and pMOB–FSI composites exhibited well-defined semicircular responses in the high-frequency region (Fig. 4a), characteristic of bulk ionic conduction within the composites. In contrast, the pMBA–PF6 and pMBA–FSI systems did not display pronounced semicircular features and instead exhibited dispersive impedance responses associated with hopping-type ionic transport.

Despite these differences in transport mechanism, all composites exhibited measurable ionic conductivity (Fig. 4b). The pMBA–PF_6, pMOB–PF_6, and pMOB–FSI systems exhibited conductivities on the order of 10^{-5}–10^{-4} S cm^{-1}. Notably, the pMBA–FSI composite displayed the highest conductivity among the investigated systems, reaching 3.7×10^{-4} S cm^{-1}. Notably, the conductivity trend does not follow ionic-liquid loading (Table S1), indicating that retained ionic-liquid content alone does not account for the observed conductivity trend. In particular, the high conductivity of pMBA–FSI is associated with its predominantly amorphous structural state.

The impedance response depends strongly on the polymer host, whereas the ionic-conductivity trend is associated with the structural state developed within the composite. Whereas the pMOB-based systems support bulk ionic conduction, the pMBA-based systems are dominated by hopping-type transport. Furthermore, the highest conductivity is observed specifically for the pMBA–FSI composite, which exhibits a predominantly amorphous PXRD profile with strongly suppressed diffraction features. This result indicates that retained ionic-liquid content alone does not account for the conductivity trend and that ionic conductivity is associated with the structural state of the composite.

The characteristic impedance responses and relative ionic-conductivity trend were retained when the electrode–sample contact load was varied from 3 N to 5 N (Table S4). These results indicate that the comparative transport behavior observed in the present series is not determined solely by the electrode–sample contact condition.

To examine whether the observed conductivity differences could be attributed simply to variations in ionic-liquid loading, the retained ionic-liquid content was subsequently estimated by thermogravimetric analysis.

5. Ionic-Liquid Content Retained in the Composites

To evaluate the amount of ionic liquid retained in the composites after methanol washing, the ionic-liquid content was estimated approximately from thermogravimetric analysis (TGA) (Figure S5). The retained ionic-liquid content was evaluated from the weight loss observed prior to the onset of significant polymer degradation (Table S1).

The results indicate that the amount of retained ionic liquid depends strongly on the polymer–ionic liquid combination. Notably, the ionic conductivity does not correlate directly with the retained ionic-liquid content. Although pMOB–FSI exhibited the highest estimated ionic-liquid content (~ 40 wt%), its ionic

conductivity (7.6×10^{-5} S cm^{-1}) was comparable to that of pMOB–PF_6 (~ 30 wt%, 8.2×10^{-5} S cm^{-1}). Conversely, pMBA–FSI exhibited an ionic conductivity approximately one order of magnitude higher than pMBA–PF_6, accompanied by a transition from a crystalline/crystalline state to a frustrated amorphous state.

These observations indicate that ionic-liquid loading alone cannot account for the conductivity differences among the composites. While the retained ionic-liquid content may contribute to the overall conductivity, the highest conductivity is observed specifically for the pMBA–FSI composite, which exhibits a predominantly amorphous PXRD profile with strongly suppressed diffraction features. This result indicates that retained ionic-liquid content alone does not account for the conductivity trend and that ionic conductivity is associated with the structural state of the composite. To obtain insight into the molecular dynamics associated with these distinct structural and transport characteristics, time-domain NMR measurements were subsequently performed.

6. Polymer Dynamic Environments Revealed by TD-NMR

Time-domain NMR (TD-NMR) measurements were performed to examine the dynamic environments of the polymer hosts used in this study (Fig. 5).

Normalized solid-echo relaxation decay curves obtained at 30°C for crystalline pMBA prepared by phase-change polymerization (pMBA-Cryst), solution-polymerized amorphous pMBA (pMBA-Amorph; intrinsic viscosity = 0.15 dL g^{-1}), and pMOB. pMOB exhibits slower relaxation than the pMBA-based polymers, indicating less constrained polymer dynamics. Quantitative relaxation parameters derived from the relaxation-component analysis are summarized in Tables S2 and S3. The observed differences suggest that the polymer hosts provide distinct dynamic environments that may influence ion-transport pathways in the corresponding polymer–ionic liquid composites.

Solid-echo relaxation decays were obtained at 30°C for crystalline pMBA (pMBA-Cryst), amorphous pMBA (pMBA-Amorph), and pMOB. The NMR relaxation behavior differed between the pMBA-based polymers and pMOB. In particular, pMOB exhibited a slower relaxation decay than either pMBA-Cryst or pMBA-Amorph, indicating less constrained polymer dynamics.

Although pMBA-Cryst and pMBA-Amorph showed broadly similar relaxation profiles, subtle differences were observed in the relative contributions of constrained and mobile components, reflecting modest changes in local polymer dynamics upon amorphization. The individual relaxation-component amplitudes used for this analysis are provided in Table S2.

Quantitative parameters extracted from the relaxation-component analysis are summarized in Table S3. The average apparent relaxation time (T_2 average) increased

in the order pMBA-Cryst < pMBA-Amorph < pMOB, whereas the average second moment (M_2average) decreased in the same order, indicating progressively reduced dynamic constraints and weaker residual

dipolar interactions from pMBA-Cryst to pMOB.

Interestingly, this trend parallels the ion-transport behavior observed in the polymer–ionic liquid composites. Electrochemical impedance spectroscopy revealed that both pMBA-based composites (pMBA–PF_6 and pMBA–FSI) exhibit hopping-type ionic transport, whereas both pMOB-based composites (pMOB–PF_6 and pMOB–FSI) show bulk ionic conduction.

Although the present TD-NMR measurements were performed on the neat polymers, the results suggest that the dynamic environments provided by the polymer hosts may influence the transport pathways available to the confined ionic liquids. The relatively less constrained dynamics of pMOB may contribute to the formation of more continuous ion-conduction pathways, whereas the more constrained environment characteristic of pMBA-based polymers may favor localized hopping transport. These observations suggest that polymer dynamics may contribute to the distinct ionic transport mechanisms observed in the corresponding polymer–ionic liquid composites.

7. Discussion

The key advance of this work is the identification of two distinct structural responses in confined polymer–ionic liquid composites, whose occurrence and ionic-conductivity trends are consistent with frustration-mediated state selection. Previous studies have shown that confinement can stabilize unusual ionic ordering, but the present comparative series identifies two distinct structural responses associated with different polymer–ionic liquid combinations. One structural response is associated with thermally persistent ordered diffraction features, whereas the other structural response is associated with strongly suppressed diffraction features and a predominantly amorphous state. The emergence of these two modes demonstrates that the structural response of confined ionic systems cannot be understood solely in terms of polymer crystallinity, ionic-liquid chemistry, or confinement in isolation, but instead arises from the way competing frustrations are resolved across the composite.

The present results reveal two distinct modes of frustration accommodation (Fig. 6).

Conceptual schematic summarizing the observed structural responses and a proposed interpretation in terms of frustration accommodation. Mode I denotes the three composites exhibiting ordered diffraction features, whereas Mode II denotes pMBA–FSI, which exhibits a predominantly amorphous diffraction profile with strongly suppressed long-range diffraction features. The observed structural states are associated with distinct ionic-conductivity responses across the present composite series.

The present study reveals that polymer–ionic liquid composites do not respond uniformly to confinement. Although all systems were prepared using the same PCP process and incorporated ionic liquids containing the same $BMIM^+$ cation, markedly different structural states emerged depending on the polymer–anion combination. Specifically, pMBA–PF_6, pMOB–PF_6, and pMOB–FSI developed ordered ionic structures, whereas pMBA–FSI remained predominantly amorphous over the entire temperature range investigated. These observations indicate that the structural response cannot be explained solely

by confinement, polymer crystallinity, or ionic-liquid chemistry individually. Instead, it emerges from the manner in which competing ordering tendencies are structurally accommodated within the composite.

Meta-linked aromatic polymers inherently impose packing constraints because their non-linear molecular topology prevents simultaneous optimization of local packing interactions. The confined ionic liquids introduce an additional source of frustration arising from charge ordering, conformational flexibility, and competing intermolecular interactions. Consequently, the composite must accommodate frustration originating from both the polymer and ionic-liquid components.

In the first mode, observed for pMBA–PF_6, pMOB–PF_6, and pMOB–FSI, ordered diffraction features are observed. The ordered diffraction features indicate the development of long-range structural order in these composites. This produces diffraction peaks that remain detectable over a broad temperature range and exhibit no evidence of major thermally induced phase transitions. In the second mode, observed exclusively for pMBA–FSI, long-range diffraction features are strongly suppressed. Although crystalline pMBA tends to form a hydrogen-bonded ordered framework, the pMBA–FSI combination does not develop the long-range diffraction order observed for the other composites. Instead, diffraction features attributable to long-range polymer crystallinity and ionic ordering are strongly suppressed, resulting in a thermally persistent predominantly amorphous state.

An important observation is that the suppression of long-range ordering cannot be attributed solely to the conformational flexibility of the FSI^- anion. Although FSI^-containing ionic liquids are generally less prone to long-range ordering than their PF_6^- counterparts, the pMOB–FSI composite nevertheless develops ordered diffraction features that persist upon heating. The emergence of the predominantly amorphous state is therefore specific to the pMBA–FSI combination and cannot be explained by anion chemistry alone. Instead, it suggests that structural-state selection arises from the particular interaction between polymer-derived and ionic-liquid-derived ordering tendencies within the confined composite.

The observed state selection can be discussed in the broader context of geometrical frustration, in which locally preferred configurations cannot be extended throughout a system because of global constraints. [21, 22] Classical geometrical frustration is typically discussed in terms of locally preferred structures that cannot be propagated into a compatible global order because of geometric constraints. In contrast, the present system may represent an inverse situation, where an already established confinement field generated by the polymer host restricts the local ordering pathways available to the confined ionic liquid. In this sense, frustration arises not only from the inability of local order to develop into global order, but also from the inability of local ordering motifs to fully adapt within an externally imposed global structural framework.

In the present composites, the coexistence of polymer-derived and ionic-liquid-derived ordering tendencies provides a possible analogue of such frustration: local packing motifs favored by the polymer and ionic-liquid components may not be simultaneously compatible within the confined composite morphology.

One possible interpretation is that the observed Mode I and Mode II responses reflect different ways of accommodating frustration arising from competing ordering tendencies within the confined composite. In the context of classical geometrical frustration, systems often develop partially ordered states because locally preferred arrangements cannot be propagated into a compatible global structure. In the present system, however, the hierarchy may be partially inverted: an already established confinement field generated by the polymer host restricts the local ordering pathways available to the confined ionic liquid. Under these conditions, frustration may be accommodated either through the emergence of ordered ionic domains (Mode I) or through suppression of long-range ordering (Mode II). In Mode I, observed for pMBA–PF_6, pMOB–PF_6, and pMOB–FSI, the system retains sufficient compatibility between polymer-derived and ionic-liquid-derived ordering tendencies to develop thermally persistent ordered diffraction features. In contrast, in Mode II, represented by pMBA–FSI, the competing ordering tendencies appear less mutually compatible, resulting in strong suppression of long-range diffraction features and the selection of a predominantly amorphous structural state. The microscopic structural origin of these distinct responses, including the role of morphology established during phase-change polymerization, remains to be established. Nevertheless, the observed coexistence of ordered and amorphous accommodation pathways is consistent with frustration-mediated structural-state selection in the present polymer–ionic liquid composites.

The absence of crystallization during VT-PXRD measurements and the lack of melting or crystallization signatures in DSC indicate that the predominantly amorphous state persists over the experimental temperature range. Furthermore, the retained ionic-liquid content estimated from thermogravimetric analysis demonstrates that ionic transport cannot be explained simply by ionic-liquid loading. Most notably, pMOB–FSI retained the largest amount of ionic liquid (~ 40 wt%) but did not exhibit the highest conductivity (7.6×10^{-5} S cm^{-1}), whereas pMBA–FSI exhibited the highest conductivity (3.7×10^{-4} S cm^{-1}) despite a lower ionic-liquid content (~ 30 wt%). Apart from the absolute conductivity values, the two distinct transport mechanisms observed in the electrochemical impedance spectroscopy results also reveal another important point. Both pMOB-based composites exhibited semicircular Nyquist responses characteristic of bulk ionic conduction whereas both pMBA-based composites displayed dispersive responses characteristic of hopping-type transport. Therefore, the superior transport behavior of pMBA–FSI is obtained in the absence of bulk ionic conduction and while simultaneously exhibiting the strongest suppression of structural ordering.

This observation is particularly notable because it challenges the conventional assumption that ionic conductivity is determined primarily by crystallinity. Whereas the ordered systems accommodated frustration through the formation of ionic domains, pMBA–FSI accommodated frustration through suppression of ordering. The latter accommodation mode appears to generate a more favorable environment for ion transport, yielding the highest conductivity among the investigated systems.

The TD-NMR results further emphasize the importance of dynamic heterogeneity in the polymer hosts. Crystalline pMBA, amorphous pMBA, and pMOB exhibited distinct relaxation behaviors despite their similar aromatic backbone structures. These observations suggest that ionic liquids are accommodated

within dynamically heterogeneous polymer environments rather than structurally uniform matrices. Such heterogeneity may influence how frustration is distributed, localized, or relaxed within the composite, thereby affecting both structural evolution and ion-transport behavior.

In summary, the present results reveal that within the present series, ionic conductivity is not explained by crystallinity or retained ionic-liquid loading alone. The results are consistent with the possibility that the manner in which competing ordering tendencies are accommodated contributes to the selected structural state and to ionic conductivity. Accordingly, two distinct modes of frustration accommodation emerge from this study: Mode I, the formation of ordered ionic domains, observed for pMBA–PF_6, pMOB–PF_6, and pMOB–FSI; and Mode II, the formation of a frustrated amorphous state, observed for pMBA–FSI. Our results show that confinement does not merely stabilize an unusual ionic phase; it can select between distinct thermally persistent structural states through the competition of polymer- and ionic-liquid-derived ordering tendencies. In the present series, suppression of long-range ordering produces the most conductive state despite its intermediate ionic-liquid content. Structural-state selection therefore provides a design principle for controlling the order–mobility trade-off in confined ionic materials.

Methods

Materials and sample preparation

3-Aminobenzoic acid and 3-hydroxybenzoic acid were purchased from Tokyo Chemical Industry Co., Ltd. (Japan). 1-Butyl-3-methylimidazolium hexafluorophosphate (BMIM–PF_6) was obtained from Sigma-Aldrich, and 1-butyl-3-methylimidazolium bis(fluorosulfonyl)imide (BMIM–FSI) was kindly supplied by Nippon Nyukazai Co., Ltd. All materials were used as received without further purification.

All polymer–ionic liquid composites were prepared by the same phase-change polymerization (PCP) procedure. Either 3-aminobenzoic acid for pMBA or 3-hydroxybenzoic acid for pMOB was dissolved in BMIM-PF_6 or BMIM-FSI at a monomer concentration of 8 wt% relative to the total mass of the monomer–ionic-liquid mixture. The mixture was heated at 200°C for 24 h under nitrogen to afford the corresponding polymer–ionic liquid composite. Using this common procedure, four composites were prepared: pMBA–PF_6, pMBA–FSI, pMOB–PF_6, and pMOB–FSI. After polymerization, each product was cooled to room temperature, collected, and washed thoroughly with hot methanol to remove unreacted monomer and non-incorporated ionic liquid. The washed powders were dried under vacuum at 200°C for 10 h before characterization. The same polymerization, washing, and drying protocol was used for all four composites unless otherwise stated. The ionic-liquid contents remaining after washing and drying were estimated by thermogravimetric analysis (TGA) as described below and are summarized in Table S1. The retention of BMIM-PF_6 in PF_6-containing composites was further confirmed by X-ray fluorescence (XRF) through the characteristic phosphorus signal (Figure S2). Incorporation of ionic-liquid-derived components in all composites was additionally examined by FT-IR spectroscopy (Figure S6).

Powder X-ray diffraction (PXRD)

PXRD measurements were carried out using a Rigaku RINT-TTR3 diffractometer with Cu Kα radiation (λ = 1.5418 Å), operated at 40 kV – 300 mA. Data were collected at room temperature over a 2θ range of 5–50°.

Variable-temperature PXRD measurements were performed under vacuum using a Rigaku SmartLab system operated at 45 kV – 200 mA with Cu Kα radiation and equipped with an Anton Paar DCS500 cooling/heating stage. The temperature was varied from 30°C to 320°C and back, and diffraction patterns were recorded at each step after thermal equilibration for 10 mins.

Differential scanning calorimetry (DSC)

DSC measurements were performed using a Mettler Toledo DSC1 instrument under a nitrogen atmosphere. Samples were heated and cooled between − 40°C and 280°C at a rate of 5°C min^{-1}.

The glass transition temperature (Tg) was determined from the midpoint of the step change in heat flow during the second heating cycle.

Thermogravimetric analysis (TGA)

TGA measurements were conducted using a Netzsch STA449 F1 instrument under argon atmosphere. Samples were heated from 25°C to 700°C at a rate of 10°C min^{-1}.The retained ionic-liquid content of each composite was estimated approximately from the weight loss observed before the onset of significant polymer degradation.

Infrared spectroscopy (FT-IR)

FT-IR spectra were recorded using a Jasco FT/IR-4100 spectrometer in transmission mode (4000–400 cm^{-1}, resolution 4 cm^{-1}, 64 scans). Powder samples were dispersed in KBr pellets. Measurements were conducted before and after thermal treatment (up to 300°C) to confirm the chemical integrity of the ionic liquid and to analyze polymer–ionic liquid interactions. Characteristic absorption bands originating from both the polymer matrix and the incorporated ionic liquids were observed, confirming successful incorporation of the ionic liquids into the composites (Figure S6).

X-ray fluorescence (XRF) spectroscopy

XRF measurements were performed using a Rigaku EDXL300 spectrometer (50 kV, 1 mA) to confirm the presence of PF_6^- in the composite.

Samples were mounted on PTFE holders with a Prolene film window and measured under vacuum at room temperature. The presence of characteristic P K-α signals was used to confirm the incorporation of BMIM-PF_6.

Spectra recorded before and after thermal treatment (300°C) showed no significant changes, indicating stable retention of the ionic liquid within the polymer matrix.

Scanning electron microscopy (SEM)

SEM observations were performed using a JEOL JSM-6701F instrument. Dry powder samples were placed on carbon-coated Cu TEM grids (ELS-C10, Okenshoji Co., Ltd.) and gently tapped to remove loose particles before loading and imaging at an acceleration voltage of 5 kV. The morphologies of the neat polymers are shown in Figure S7 for comparison.

Time-domain NMR (TD-NMR)

TD-NMR measurements were carried out to evaluate the dynamic environments of the polymers, a method widely used to investigate molecular mobility and dynamic constraints in soft matter systems. [26–28] Measurements were performed using NMR analyzer Spin Track (Resonance Systems GmbH, Kirchheim unter Teck, Germany).

Solid-echo relaxation decays were recorded at 30°C for crystalline pMBA (pMBA-Cryst), amorphous pMBA (pMBA-Amorph), and pMOB. The pMBA-Amorph sample was prepared by solution polymerization and used as an amorphous reference possessing the same polymer backbone as pMBA-Cryst. The intrinsic viscosities of pMBA-Cryst and pMBA-Amorph were 0.28 and 0.15 dL g^{-1}, respectively. The TD-NMR comparison was therefore intended to evaluate differences in dynamic environments associated primarily with structural state rather than to provide a quantitative assessment of molecular-weight effects.

The relaxation curves were analyzed using a multi-component relaxation model consisting of short-, middle-, and long-relaxation components. Since the decays exhibited oscillatory features characteristic of glassy and/or crystalline polymers, the solid-like components (short and middle) were described using two Pake functions [28], whereas the mobile fraction (long component) was fitted using a stretched exponential function. The apparent relaxation time T_2^* for each of the contributing decays was calculated based on the second moment Gaussian approximation $T_2^* = \sqrt{\frac{2}{M_2}}$ while the values of M_2 in μs^{-2} were obtained from the fitting procedure implemented in the Spin Track analysis software. The relative amplitude (a) and apparent transverse relaxation time (T_2) of each component were determined from the fitting procedure.

From the fitted parameters, average apparent relaxation times (T_2 average) and average second moments (M_2 average) were calculated to provide semi-quantitative measures of molecular mobility and dynamic constraints. Larger T_2 average values indicate less constrained molecular motion, whereas larger M_2 average values correspond to stronger residual dipolar interactions and greater dynamic constraint.

The TD-NMR analysis was used to compare the dynamic environments of the polymer hosts and to evaluate possible relationships between polymer dynamics and ionic transport behavior in the corresponding polymer–ionic liquid composites.

Electrochemical impedance spectroscopy (EIS)

EIS measurements were performed on compression-molded composite sheets. The samples were prepared as circular films with a diameter of 10 mm and a thickness of 0.4–0.5 mm by hot pressing at 260°C under a uniaxial load of approximately 12 kN for 5 min.

To confirm that hot pressing did not alter the structural state of the composites, PXRD patterns were measured before and after hot pressing at 260°C. No substantial changes in the diffraction profiles were observed for any composite, including the predominantly amorphous pMBA–FSI sample. These results indicate that the long-range structural characteristics resolved by PXRD were retained during preparation of the EIS specimens.

Measurements were carried out using stainless-steel blocking electrodes over the frequency range from 1 MHz to 10 mHz with an AC amplitude of 10 mV at 30°C. To examine the robustness of the impedance response against electrode–sample contact conditions, EIS measurements were conducted using contact loads of 3 N and 5 N. The characteristic impedance responses and the relative ionic-conductivity trend among the composite formulations were preserved under both contact-load conditions. The conductivity values reported in the main text were obtained at a contact load of 5 N, unless otherwise stated.

Reproducibility

The structural and thermal characterizations were repeated using at least two independently prepared batches to confirm reproducibility. In independent preparations, pMBA–PF_6, pMOB–PF_6, and pMOB–FSI consistently exhibited ordered diffraction features, whereas pMBA–FSI consistently exhibited a predominantly amorphous diffraction profile with strongly suppressed diffraction features. For EIS, the influence of electrode–sample contact conditions was assessed by performing measurements at contact loads of 3 N and 5 N. Although the absolute impedance values depended on contact conditions, the qualitative impedance responses and the relative ionic-conductivity trend among the four composites were maintained under both conditions.

Declarations

Competing Interests

S.O. is an inventor on a patent application related to the materials described in this work. All other authors declare no competing interests.

Funding

This work was supported by the RIKEN–Sumitomo Chemical collaborative research program.

Author Contributions

S.O. conceived and supervised the project. S.O., J.L., J.I., and L.G. designed the experiments and analyzed the data. S.O. performed the synthesis. J.L. conducted the structural characterization. J.I. performed the TD-NMR measurements. L.G. performed the TD-NMR data analysis and interpretation. S.O. wrote the manuscript with input from all authors. All authors discussed the results and contributed to the final version of the manuscript.

Acknowledgements

We gratefully acknowledge Professor Junji Watanabe for his insightful advice encouraging us to explore structure formation in polymers, which significantly influenced the direction of this study. We also thank Dr. Kiyohiro Adachi and Dr. Michiko Tanaka for their valuable assistance with X-ray diffraction (XRD) and X-ray fluorescence (XRF) measurements, respectively. We thank Gurvan Bosser for his valuable assistance with powder X-ray diffraction (pXRD) and Ying Feng and Kuniyo Yamada for their kind help with FT-IR measurements. We thank JFE Techno-Research Corporation for technical support in electrochemical impedance measurements. We gratefully acknowledge Mageleka Japan Co., Ltd. for technical support with the TD-NMR measurements. We also gratefully acknowledge Nippon Nyukazai Co., Ltd. for kindly providing BMIM–FSI.

Data Availability

All data supporting the findings of this study are available within the article and its Supplementary Information files. Additional raw data are available from the corresponding author upon reasonable request.

References

1. Plechkova AE, Seddon KR (2008) Applications of ionic liquids in the chemical industry. Chem Soc Rev 37:123–150

2. Hayes R, Warr GG, Atkin R (2015) Structure and nanostructure in ionic liquids. Chem Rev 115:6357–6426
3. Armand M, Endres F, MacFarlane DR, Ohno H, Scrosati B (2009) Ionic-liquid materials for the electrochemical challenges of the future. Nat Mater 8:621–629
4. Tokuda H, Hayamizu K, Ishii K, Susan MABH, Watanabe M (2004) Physicochemical properties of room temperature ionic liquids: 1. Viscosity, conductivity, and surface tension of 1-alkyl-3-methylimidazolium hexafluorophosphate and hexafluoroborate. J Phys Chem B 108:16593–16600
5. Wasserscheid P, Welton T (eds) (2008) Ionic Liquids in Synthesis, 2 edn. Wiley-VCH, Weinheim
6. Dupont J, de Souza RF, Suarez PA (2002) Z. Ionic liquid (molten salt) phase organometallic catalysis. Chem Rev 102:3667–3692
7. MacFarlane DR et al (2016) The future of ionic-liquid research: translating fundamentals to applications. Nat Rev Mater 1:15005
8. Zhu H, MacFarlane DR, Pringle JM, Forsyth M (2019) Ionic liquid electrolytes for future energy storage technologies. Trends Chem 1:126–140
9. Thomas ML, Hatakeyama-Sato K, Nanbu S, Yoshizawa-Fujita M (2023) Ionic liquids for advanced energy applications. Energy Adv 2:748–764
10. Alcoutlabi M, McKenna GB (2005) Effects of confinement on material behaviour at the nanometre size scale. J Phys : Condens Matter 17:R461–R524
11. Lotz B, Cheng SZ (2008) D. Polymer crystallization processes as seen from the growth front's perspective. Polym J 40:891–899
12. Guo D-S, Liu Y (2012) Calixarene-based supramolecular polymerization in solution. Chem Soc Rev 41:5907–5921
13. Huber P (2015) Soft matter in hard confinement: phase transition thermodynamics, structure, texture, diffusion and flow in nanoporous media. J Phys : Condens Matter 27:103102
14. He Y, Khan MA, Drake AD, Garay J, Shirodkar A, Goodlett S, Strzalka J, Ladipo F, Knutson BL, Rankin SE (2025) Crystallization of nanopore-confined imidazolium ionic liquids probed by temperature-resolved in situ grazing-incidence wide angle X-ray scattering (GIWAXS). Nanoscale Adv 7:6607–6619
15. Borghi F, Podestà A (2020) Frustrated interfaces: how competing interactions shape wetting, adhesion and friction at the nanoscale. Adv Phys X 5:1736949
16. Chen S, Wu G, Sha M, Huang S (2007) Ionic liquids confined in nanoporous carbon: phase behavior and ionic ordering. J Am Chem Soc 129:2416–2417
17. Wang S, Liu Z, Li Y, Chen H, Zhang J (2025) Confinement-induced ionic superlattices in nanoporous crystals. Nat Commun 16:9007
18. Okamoto S, Llandro J (2026) Topology controlled frustrated solid state of ionic liquids without a detectable melting transition. Research Square Preprint. https://doi.org/10.21203/rs.3.rs-10321809/v1

19. Huang J, Zhou H, Zhang L, Zhang L, Shi W, Yang Y, Zhou J, Zhao T, Liu M (2025) Nanotetrapods Promote Polymer Flow Through Confinement-Induced Packing Frustration. Nat Commun 16:8550
20. Huang J, Zhou H, Zhang L, Zhang L, Shi W, Yang Y, Zhou J, Zhao T, Liu M (2024) Full-Scale Polymer Relaxation Induced by Single-Chain Confinement Enhances Mechanical Stability of Nanocomposites. Nat Commun 15:6747
21. Sadoc JF, Mosseri R (1999) Geometrical Frustration. Cambridge University Press
22. Nelson DR (2002) Defects and Geometry in Condensed Matter Physics. Cambridge University Press
23. Okamoto S, Llandro J, Gibbons A, Arfaoui M, Hashizume D, Watanabe J (2026) Orthogonal staggered alignment of molecular chains in aramid whiskers: a game-changer for sustainable, high-performance composites. Macromol Rapid Commun 47:e00919
24. Okamoto S, Llandro J, Ikeda J, Watanabe J (2026) Perpendicular chain orientation in poly(para-benzamide) single-crystal nanowhiskers for enhanced dispersibility. ACS Appl Nano Mater 9:7330–7338
25. Okamoto S, Llandro J, Teng K-F, Chang P, Liang K, Arfaoui M, Hashizume D, Watanabe J (2026) Microbially derived p-aminobenzoic acid for poly(p-benzamide) whiskers: the influence of monomer synthetic routes on crystallization and thermal behavior. React Funct Polym 227:106868
26. Ikeda J (2022) Effects of processing conditions on microstructure and mechanical properties of powder-metallurgy steels. *J. Jpn. Soc. Powder Metall.* 69, 484–489 [27] Kuzu, S. NMR characterization of microstructure and water dynamics in food materials. *J. Sci. Food Agric.* 105, 489–497 (2025)
27. Grunin L, Ivanova M, Schiraya V, Grunina T (2023) Advanced time-domain NMR methods for probing molecular dynamics in soft matter. Appl Magn Reson 54:929–955
28. Barsoukov E, Macdonald JR (eds) (2005) Impedance Spectroscopy: Theory, Experiment, and Applications, 2 edn. Wiley
29. Yang M, Epps TH (2026) III. Block polymer electrolytes: nanostructure, ion transport and solid-state battery applications. Polym Chem 17:971–983
30. Shao Y, Gudla H, Mindemark J, Brandell D, Zhang C (2024) Design principles for solid polymer electrolytes: interfaces, ion transport and mechanical stability. Acc Chem Res 57:1123–1134

Figures

a)

	Ionic Liquid	
	BMIM PF_6 (Ordering-prone)	BMIM FSI (Frustration-prone)
Polymer		
pMBA (Crystalline)	pMBA-PF_6	pMBA-FSI
pMOB (Amorphous)	pMOB-PF_6	pMOB-FSI

b)

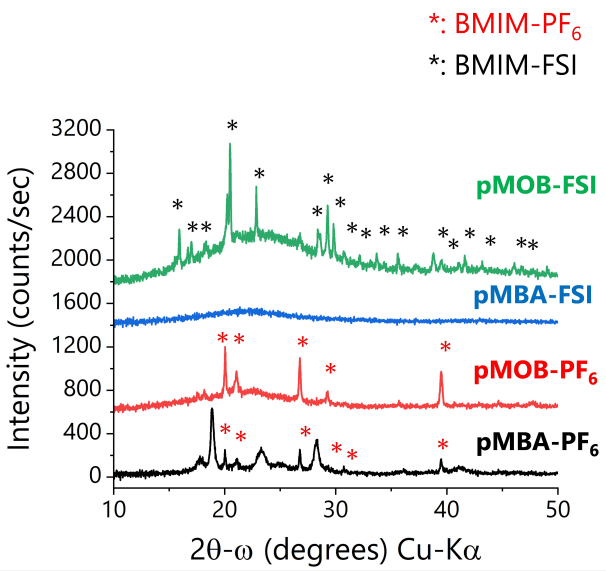


Figure 1

Design and structural responses of polymer–ionic liquid composites.

(a) Four model polymer–ionic liquid composites prepared by phase-change polymerization (PCP) using crystalline poly(m-benzamide) (pMBA) and amorphous poly(m-oxybenzoate) (pMOB) as polymer matrices and 1-butyl-3-methylimidazolium (BMIM)-based ionic liquids containing PF_6^- and FSI^- anions. The composites were obtained by polymerization at 200 °C for 24 h, followed by methanol washing and vacuum drying.

(b) Room-temperature PXRD patterns of pMBA–PF_6, pMOB–PF_6, pMBA–FSI, and pMOB–FSI. Distinct diffraction peaks are observed for pMBA–PF_6, pMOB–PF_6, and pMOB–FSI, indicating the development of ordered structures within the composites. In contrast, pMBA–FSI exhibits a broad diffraction profile with substantially suppressed diffraction features, demonstrating a markedly different structural response from the other three systems.

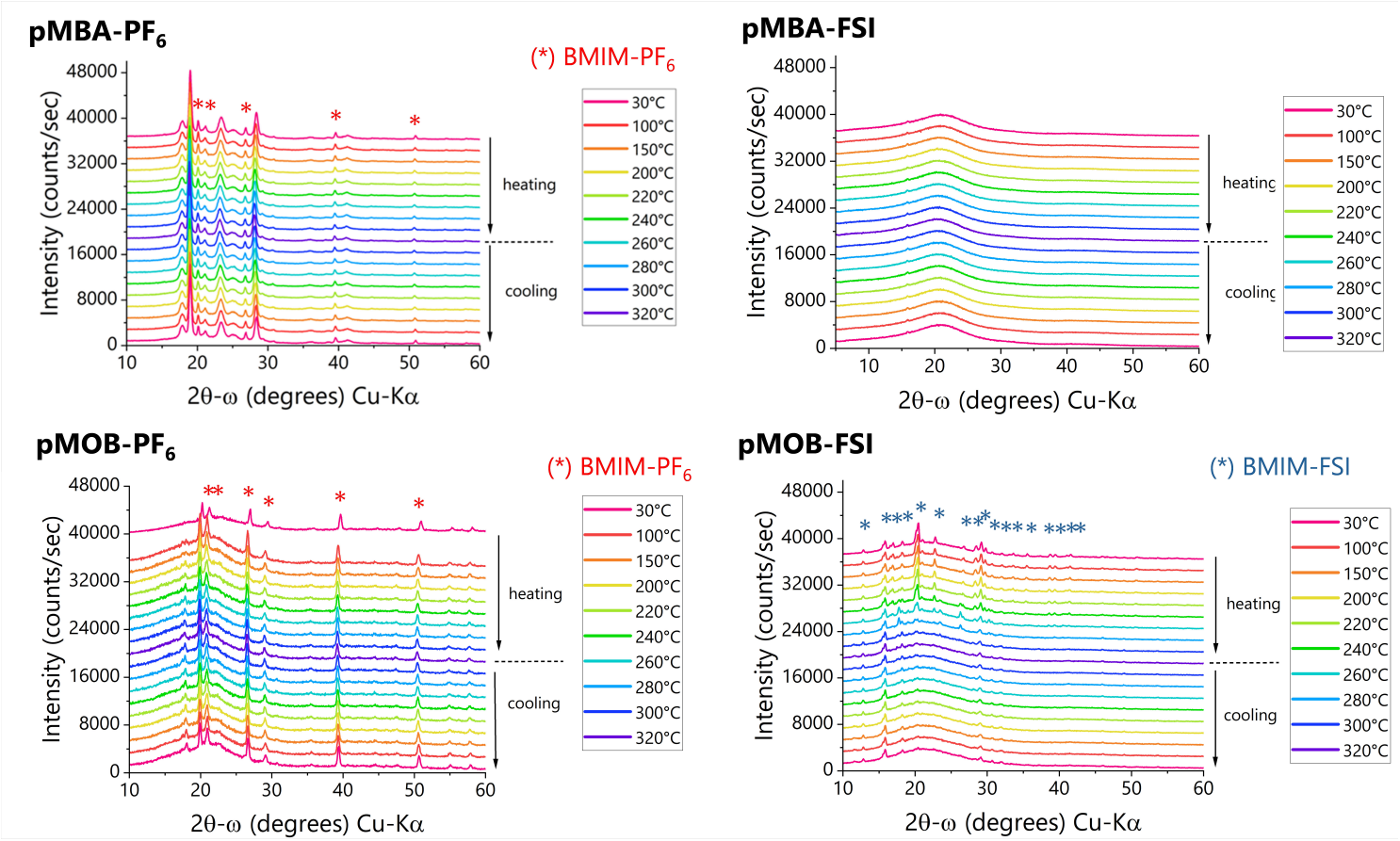


Figure 2

Thermal persistence of ordered and amorphous structural states in polymer–ionic liquid composites.

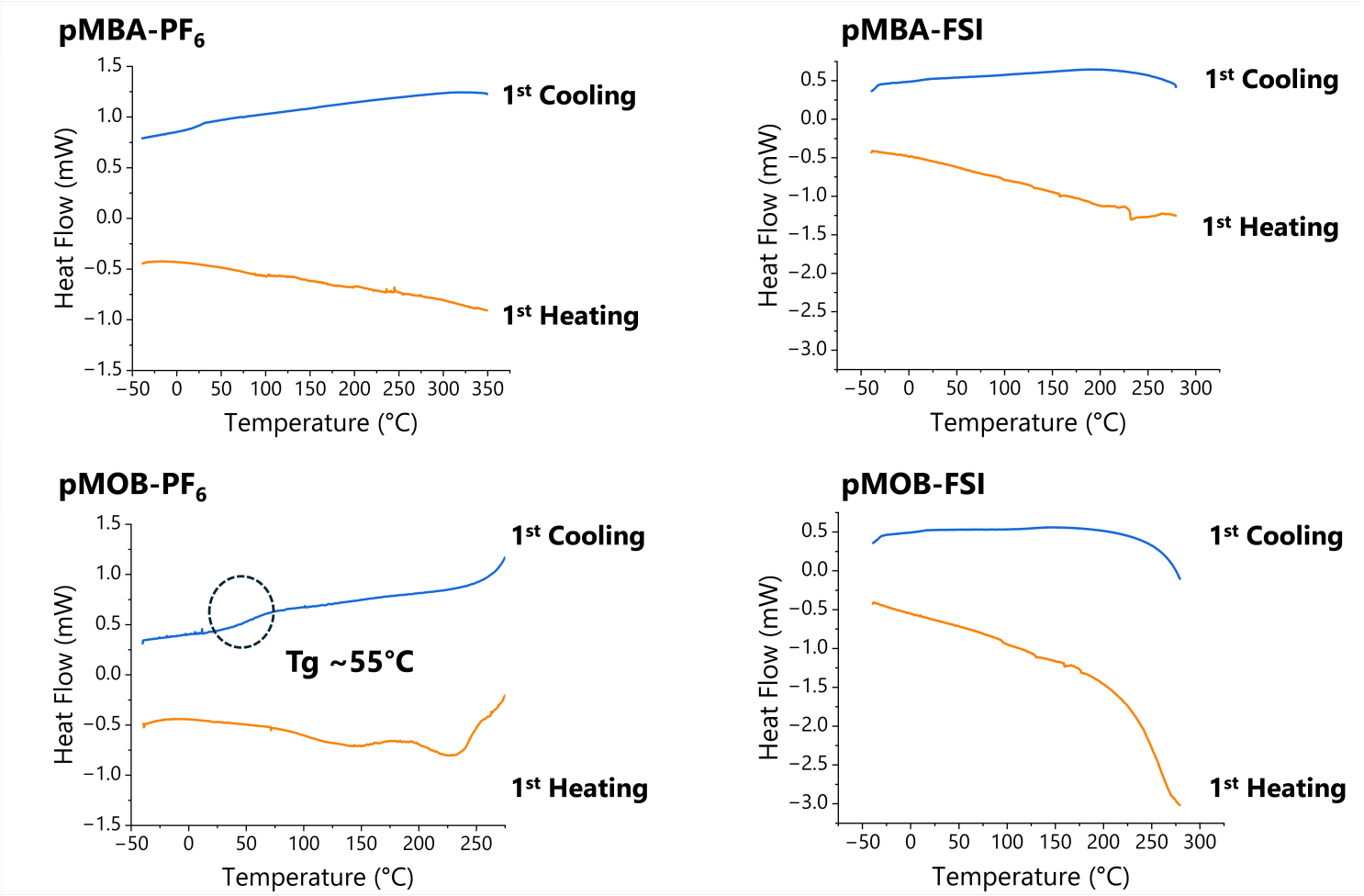


Figure 3

Thermal behavior of structurally distinct polymer–ionic liquid composites.

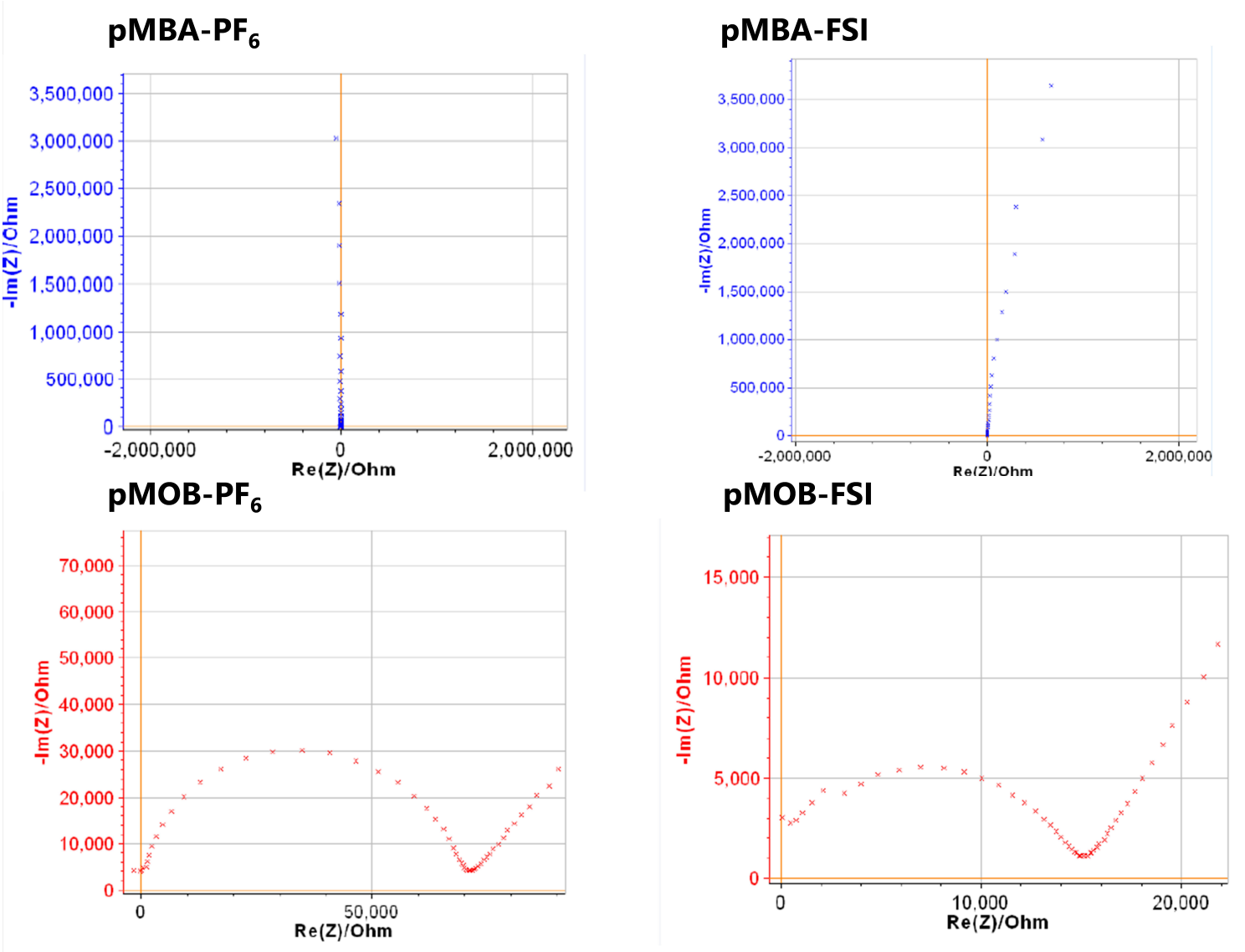


Figure 4

Ionic transport behavior of polymer–ionic liquid composites.

(a) Nyquist plots obtained from electrochemical impedance spectroscopy (EIS) measurements of pMBA–PF_6, pMOB–PF_6, pMBA–FSI, and pMOB–FSI at 30 °C. The pMOB-based composites exhibit well-defined semicircular responses characteristic of bulk ionic conduction, whereas the pMBA-based composites display dispersive responses associated with hopping-type transport.

(b) Ionic conductivities of the corresponding composites measured at 30 °C. The pMBA–PF_6, pMOB–PF_6, and pMOB–FSI systems exhibit ionic conductivities on the order of 10^{-5}–10^{-4} S cm^{-1}, while the pMBA–FSI composite reaches 3.7×10^{-4} S cm^{-1}.

These results demonstrate that ionic conductivity and impedance response vary strongly among the polymer--ionic liquid composites. The impedance response depends strongly on the polymer host,

whereas the ionic-conductivity trend is associated with the structural state developed within the composite.

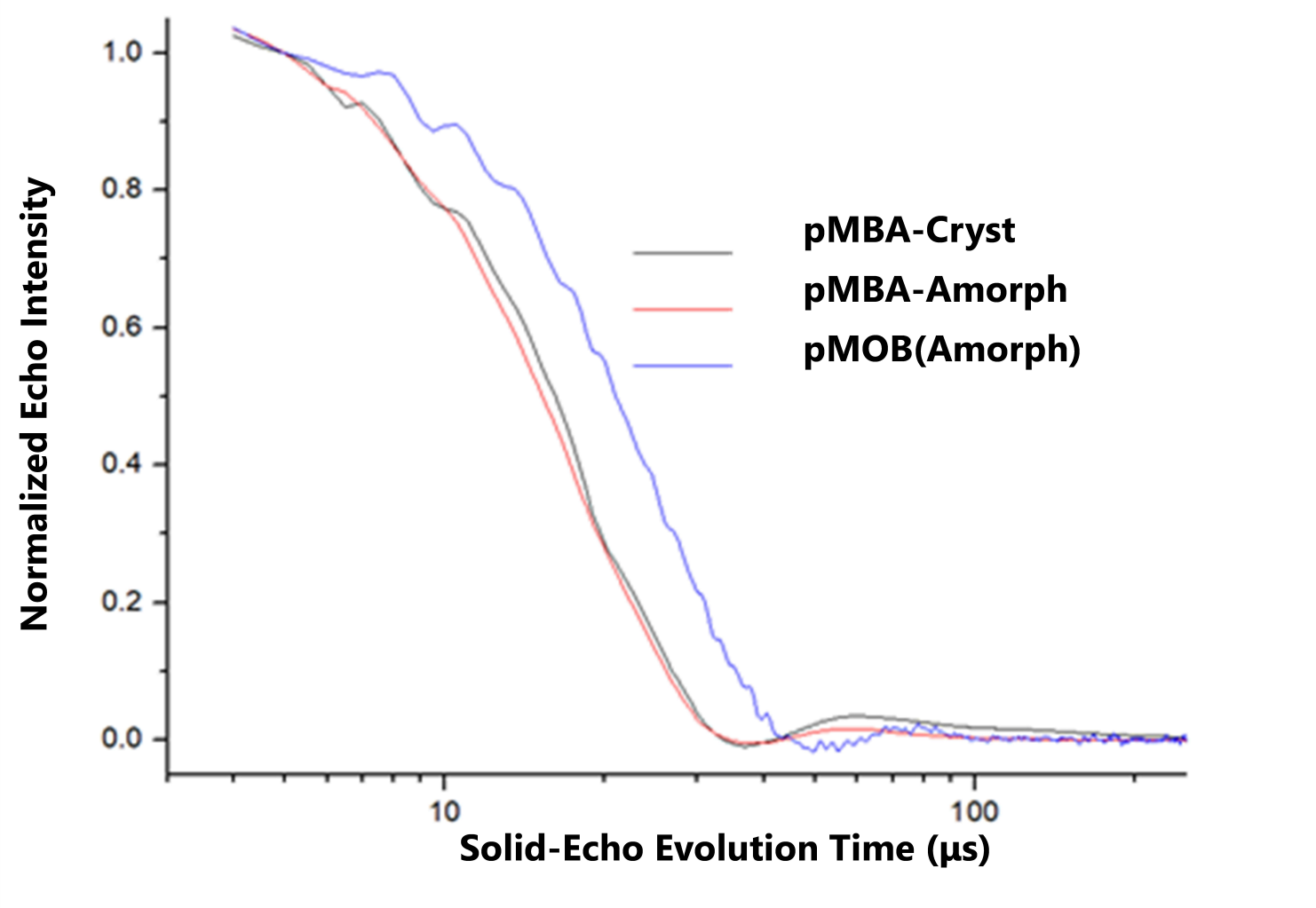


Figure 5

TD-NMR relaxation behavior of meta-linked aromatic polymers.

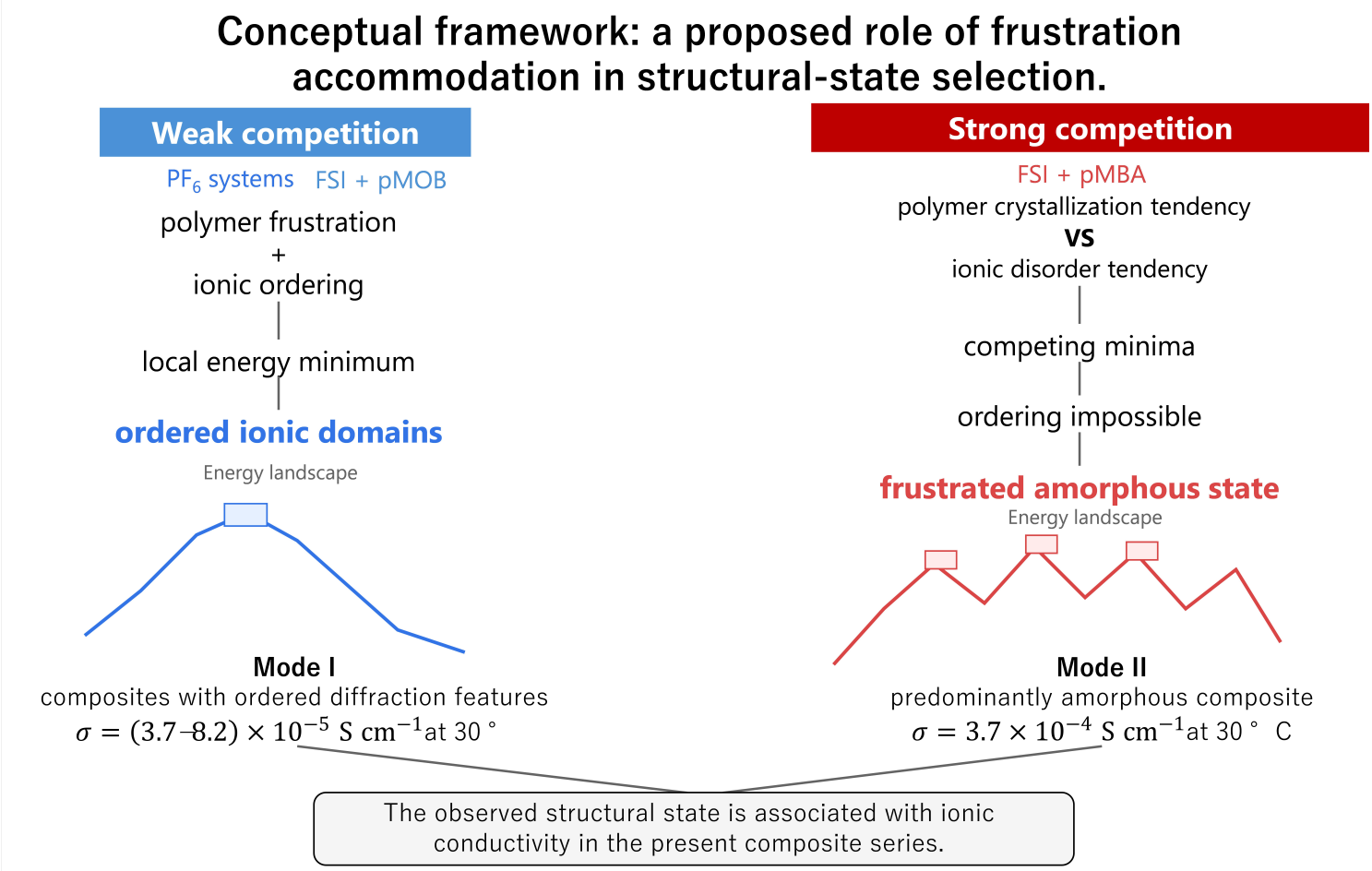


Figure 6

Frustration-mediated state selection in polymer–ionic liquid composites.

Supplementary Files

This is a list of supplementary files associated with this preprint. Click to download.

- SupportingInformation.docx
- Preprint.pdf